Check for updates

Proceedings of ASME Turbo Expo 2018
Turbomachinery Technical Conference and Exposition
GT2018
June 11-15, 2018, Oslo, Norway

GT2018-75369

Downloaded from https://asmedigitalcollection.asme.org/GT/proceedings-pdf/GT2018/50985/V001T09A002/3768152/v001t09a002-gt2018-75369.pdf by guest on 21 July 2020

OPTIMISED TEST RIG FOR MEASUREMENTS OF AERODYNAMIC AND AEROACOUSTIC PERFORMANCE OF LEADING EDGE SERRATIONS IN LOW-SPEED FAN APPLICATION

Till M. Biedermann
Institute of Sound and Vibration Engineering
ISAVE
Faculty of Mechanical and Process Engineering
University of Applied Sciences Duesseldorf
Duesseldorf, Germany

F. Kameier
Institute of Sound and Vibration Engineering
ISAVE
Faculty of Mechanical and Process Engineering
University of Applied Sciences Duesseldorf
Duesseldorf, Germany

C. O. Paschereit
Institute of Fluid Dynamics and Technical Acoustics ISTA
Faculty of Mechanical Engineering and Transport Systems,
Technical University of Berlin,
Berlin, Germany

ABSTRACT

With the aim of analysing the efficiency of leading edge serrations under realistic conditions, an experimental rig was developed where a ducted low-speed fan is installed that allows to gather data of both, aerodynamic and aeroacoustic nature. Turbulent inflow conditions were generated via biplane-square grids, resulting in turbulence intensities of different magnitude and of high isotropic character that were quantified by use of hot-wire measurements. The fan blades were designed according to the NACA65(12)-10 profile with interchangeable features and an independently adjustable angle of attack. Altogether, five different parameters can be analysed, namely the serration amplitude and wavelength, the angle of attack, the inflow turbulence and the rotational speed. In addition, the blade design allows for a variation of the blade skew, sweep and dihedral as well. The presented work focusses on validating and optimising the test rig as well as a detailed quantification of the turbulent inflow conditions. Furthermore, first aerodynamic and aeroacoustic results of fan blades with straight leading edges are compared to those of serrated leading edges. The aerodynamic performance was found to be mainly affected by the serrations as a function of the serration amplitude. Aeroacoustically, a clear sensitivity towards different incoming turbulence intensities and serration parameters was detected, showing significant broadband noise reduction below 2 kHz with an overall noise reduction of ΔOASPL = 3.4 dB at maximum serration amplitudes and minimum wavelengths.

INTRODUCTION

At high-turbulent inflow conditions, the blades of axial fans are known to emit a significantly increased amount of leading edge broadband noise due to the impingement of turbulent structures on the solid surface [1]. Recent research has firmly confirmed leading edge serrations to be an effective passive treatment in both, noise reduction and in increasing specific parameters of the aerodynamic performance such as a delayed stall and high post-stall performance [2–5]. The commonly used scales of importance are depicted in Figure 1, where the peak-to-trough value is defined as amplitude A and the distance between two serration roots as the wavelength λ. Up to now, leading edge serrations are mainly analysed in wind tunnel experiments where rigidly mounted aerofoils are tested. In preliminary studies Biedermann et al. analysed a NACA65(12)-10 aerofoil with and without sinusoidal leading edge serrations both, aeroacoustically and aerodynamically by use of experimental and numerical approaches [2,6,7]. A statistical-empirical model was developed to predict the broadband noise emissions by taking into account the chord based Reynolds number, the incoming turbulence intensity, the angle of attack as well as the serration parameters amplitude and wavelength. A clear ranking of the main influencing factors could be shown and, moreover, significant interdependencies between the influencing parameters could be detected as well. As Figure 2 shows, the Reynolds number (Re) and the freestream turbulence intensity (Tu) are identified to be the main contributors to the broadband noise emissions. With the

 Copyright © 2018 ASME

aim of reducing the noise level, the serration amplitude (A/C), followed by the serration wavelength (λ/C) are the most powerful parameters.

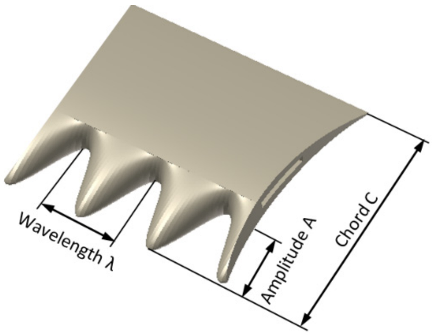

FIG. 1 SERRATED ROTOR BLADE INCLUDING MEASURES OF IMPORTANCE

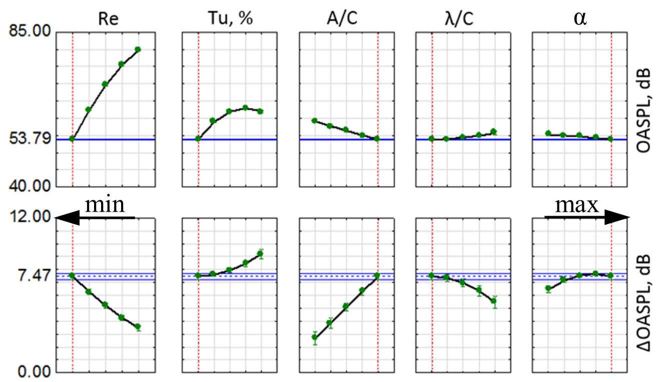

FIG. 2 EFFECTS OF INFLUENCING FACTORS ON NOISE RADIATION OASPL AND REDUCTION ΔOASPL OF RIGID SERRATED NACA65(12)-10 AEROFOIL [4]. X-AXIS: VARYATION OF EACH FACTOR FROM MIN TO MAX.

Aerodynamically, leading edge serrations have been shown to delay the stall angle and therefore enable higher maximum angles of attack [3]. In the current design, the serrations are cut into the main body, keeping the maximum chord at a constant level but suffering a loss in effective surface area. Numerically, a three-dimensional separation process as a function of the serration parameters could be extracted which highly effects the aerodynamic performance of the aerofoil [6].

Eventually, sinusoidal leading edge serrations are intended to be implemented in rotating systems such as counter-rotating rotors, compressors or turbomachines. However, recently only little research in this direction has been carried out. Zenger et al. [1] analysed the influence of distorted inflow conditions on the noise radiation of forward and backward-skewed low-pressure axial fans, using a standardised test chamber according to ISO 5801 [8]. Moreover, they also investigated sinusoidal leading edge serrations on a more rudimentary level and found only little noise reduction at the operation point whereas a significant reduction at high flow rates was achieved [9]. The aerodynamic performance, however, is not reported to be affected by large margins. Corsini et al. [10] carried out a numerical study on the influence of sinusoidal leading edge serrations or leading edge bumps in the blade tip region, which focused on the aerodynamic stall-resistance improvement.

Up to now, no combined test rig is available which allows for simultaneous measurement of aerodynamic and aeroacoustic performance while generating near isotropic turbulence and analysing already rigidly analysed aerofoils in order to draw direct conclusions on the transfer between the rigid and rotating system. The aim of the full project is to successively increase the complexity of the rotor blades step-by-step to enable a systematic analysis of the serration effects. As a first Proof-Of-Concept for the current study, straight blades were chosen, scaled according to the required maximum chord length and implemented in a rotating setup. Blade parameters such as the blade sweep, shroud and dihedral are to be analysed in subsequent settings.

TEST SETUP

A test rig according to ISO 5136 - *Determination of sound power radiated into a duct by fans and other air-moving devices – In-duct method (ISO 5136:2003)* [11] was adopted (Figure 3), where the fan is mounted in a duct of D = 0.4 m in diameter which allows for a simultaneous characterisation of the fan in terms of aeroacoustics and aerodynamics. The standardised bellmouth accounts for smooth inflow conditions, followed by a muffler to dampen the suction side noise. Subsequently, the determination of the free stream velocity, leading to the flow rate, takes place via a pitot tube or an eight-path ultrasonic volume flow analyser, respectively. At a distance of 0.8 m (x/D = 2) upstream of the mounted fan, six pressure-tabbing points are located, leading to the physically averaged suction-side pressure. The discharge pressure, however is obtained after the spin has been converted into pressure energy by a star-type flow straightener according to ISO 5801 [8]. As the acoustic measurements are taking place downstream of the fan, a semi-anechoic termination is implemented, preventing back-reflections due to impedance differences at the duct ending. Finally, an automatically driven throttling cone allows for changing the point of operation. In total, the length of the setup sums up to x/D = 30. Deviating from the ISO 5136 standard, coarse grids (turbulence grids) needed to be implemented as sources for the broadband leading edge noise of the fan, which is of essential interest in the current study. This took place x/D = 0.75 upstream of the fan, where grids of specific parameters are implemented as will be discussed in more detail in section *Turbulence*.

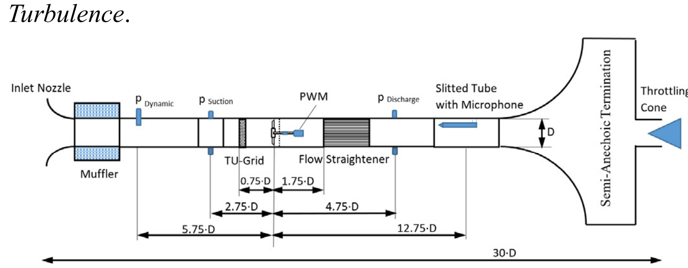

FIG. 3 ADOPTED TEST RIG ACCORDING TO ISO 5136 [8].

Downloaded from https://asmedigitalcollection.asme.org/GT/proceedings-pdf/GT2018/50985/V001T09A002/3768152/v001t09a002-gt2018-75369.pdf by guest on 21 July 2020

Copyright © 2018 ASME

In order to cover the acoustic characteristics a ½-inch B&K 4133 condenser microphone was used in a B&K UA0463 turbulence screen, featuring high degree turbulence noise suppression and which is especially constructed for measurement of airborne noise in air ducts. The turbulence screen is mounted in-line with the duct at a distance of 0.04 m from the wall. A sampling rate of SR = 44.1 kHz and a blocksize of BS = 32768 yield a frequency resolution of Δf = 1.34 Hz. Applying Hanning window and an overlapping of 66% results in a number of 240 averaged blocks during the measurement time of 60 seconds.

ROTOR DESIGN & MOUNTING

Recently, the NACA(65)12-10 aerofoil was the object of interest in a number of extensive studies on the noise reduction capabilities of serrated leading edges but limited to rigidly mounted settings [2–5]. With the purpose of analysing the transfer process of these passive noise reduction devices to the rotating setting, the same aerofoil type was used for the design of the test rotor. NACA65(12)-10 aerofoils exhibit maximum thickness of 10% relative to the chord length and are known as high-lift aerofoils, commonly used in compressors and turbines. The aim of the full project is to successively increase the complexity of the rotor blades step-by-step to enable a systematic analysis of the serration effects. As a first *Proof-Of-Concept* for the current study, straight blades were chosen, scaled according to the required maximum chord length and implemented in a rotating setup. Blade parameters such as the blade sweep, shroud and dihedral are to be analysed in subsequent settings. The design of the rotor took place according to the isolated aerofoil approach [12,13], where low solidity blading with large circumferential blade spacing is required to neglect interaction of the blades. The solidity is defined as the quotient of chord and pitch. An invisible rotor or a negligible blade interaction, respectively, can be assumed at low solidities $C/t < 0.7$ [12]. With a number of six blades, the solidity turns out to be $\sigma = 0.36$ for the blade tip and $\sigma = 0.72$ for the hub region.

$$\sigma = \frac{C}{t} \tag{1}$$

Albeit the final rotor design allows for a continuous change of the blade angle, the current flow angle of the blade was chosen to be according to the velocity triangle (Figure 4) to guarantee a blade-congruent inflow condition, considering the averaged circumferential velocity U. Eventually, the stagger angle can be determined as the sum of flow angle and angle of attack, which itself was chosen based on the maximum lift-to-drag ratio of the experimentally and numerically analysed rigid aerofoils [3,6]. For this *Proof-of-Concept* the blade chord and the blade angle were held constant. The chosen parameters yield a design point defined by a flow rate of $Q = 1.37\ m^3s^{-1}$ at a pressure rise of Δp = 108 Pa.

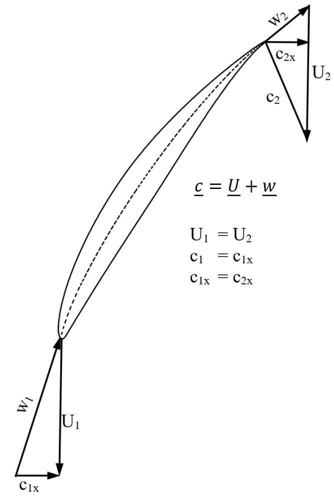

FIG. 4 VELOCITY TRIANGLE AT NACA65(12)-10 AEROFOIL TO DETERMINE THE FLOW ANGLE AT BLADE-CONGRUENT INFLOW CONDITIONS

For the experimental approach, a rotor is required that allows for a variation of multiple parameters to analyse the aeroacoustic and aerodynamic performance. The power unit consists of a high-performance PWM driven (pulse width modulated) e-motor that is commonly used in the automotive industry as it guarantees minimum self-noise as well as small installation dimension and low weight. The hub was designed to be 0.2 m in diameter, resulting in fan blades of 0.1m in span. The most important feature of the fan design is the interchangeability of the blades, leading to cost-effective possibilities of analysing blades of various geometries. As Figure 5 depicts, the blades exhibit a steel core, which provides additional stability and allows a non-positive mounting to the hub section via rotatable inserts. The bearing-mounted inserts itself allow for a continuous variation of the stagger angle, measured by use of a gauge with an accuracy of $\alpha = \pm 0.5$ deg. Thus, blades of higher complexity can easily substitute the initially analysed straight blades.

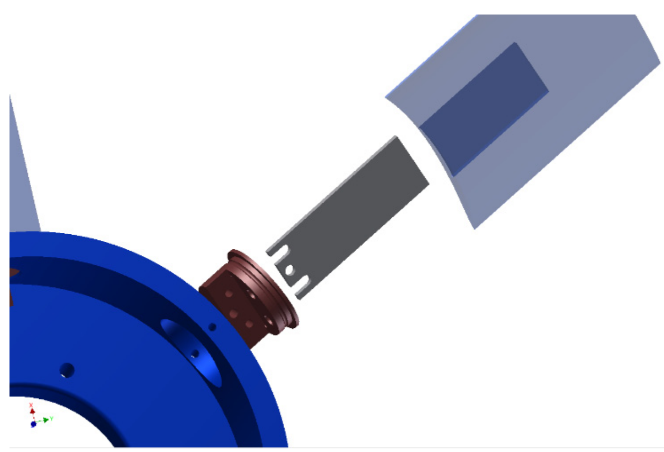

FIG. 5 MOUNTING OF INSERTS, REINFORCING STEEL PLATES AND ROTOR BLADES TO THE HUB WHILE GUARANTEEING ADJUSTABLE BLADE ANGLES.

Downloaded from https://asmedigitalcollection.asme.org/GT/proceedings-pdf/GT2018/50985/V001T09A002/3768152/v001t09a002-gt2018-75369.pdf by guest on 21 July 2020

Copyright © 2018 ASME

The rotor was decided to be manufactured via rapid prototyping, where *Alumide*, an amalgam of Polyamide and 12% of aluminium powder, was chosen as the appropriate material. With the purpose of obtaining information on the feasibility of the chosen manufacturing method and chosen material a preliminary FEM analysis has been performed by use of the FEA tool ANSYS Mechanical. Polyamide with a density of 1.13 $kg \cdot m^{-3}$ and an E-Module of 1.65 GPa was tested. An unstructured mesh with adaptive mesh refinement was used where the characteristic length of the elements ranged between $1 \cdot 10^{-5}$ m for the blade region and $6 \cdot 10^{-3}$ m for the hub, yielding a total of $2.41 \cdot 10^{5}$ elements. The spindle support of the rotor was defined to be fixed while a ramped rotation of 251 rad/s or 2400 min^{-1}, respectively, was applied. The maximum equivalent stress calculated was $\sigma_E = 2.37$ MPa at the intersection of the blades at mid-chord and the hub of the rotor while a maximum deformation of $\Delta l = 1.35 \cdot 10^{-5}$ m was obtained at the blade tips as it is exemplarily shown in Figure 6.

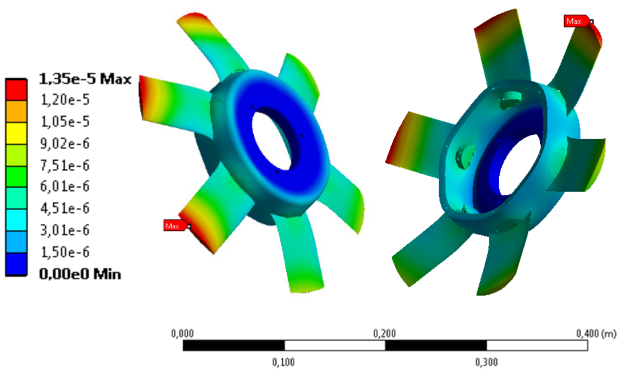

FIG. 6 STATIC-MECHANICAL ANALYSIS, TOTAL DEFORMATION[m], 2400 MIN^{-1}, BASELINE ROTOR CASE

Rotor and e-motor were mounted on a spindle where special care was directed towards the number and location of the struts. Four M8 threaded rods run through the hollow fan spindle, each forming two struts which were, for stability reasons, additionally supported by small steel tubes and fixed via locknuts on the outside of the duct. In order to prevent the transfer of solid-borne sound, shock absorbers were mounted between duct and fastening. The first set of struts was mounted 0.2 m (x/D = 0.5), the second set x/D = 1 downstream of the fan. The distance between rotor and struts has been maximised in order to reduce effects of rotor-strut-interaction to a minimum. All struts were, in addition, equipped with Scruton wires to supress possibly occurring periodic vortex shedding. The rotational speed of the rotor was obtained by use of an triaxial acceleration sensor on the fan spindle, representing a minimal-invasive high-resolution method while, in addition, providing information on the caused vibrations of the system. The signal was analysed in the frequency domain at a frequency resolution of $\Delta f = 0.25$ Hz, giving a measurement accuracy of $\pm$ 7.5 min^{-1}.

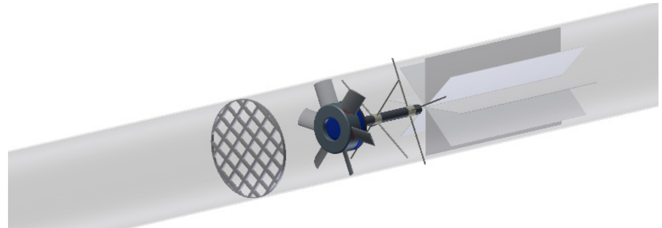

FIG. 7 DUCT-MOUNTED FAN ASSEMBLY, INCLUDING TURBULENCE GRID, ROTOR PROTOTYPE WITH PWM E-MOTOR, STATOR DESIGN AND FLOW STRAIGHTENER.

TURBULENCE

The presented study focusses on turbulence-generated aerofoil gust interaction noise, where the leading edge noise of the rotor blades is expected to represent the dominant noise source [14–16]. Hence, a high level of turbulence is required. Recent studies and noise prediction models usually refer to turbulence of isotropic or near-isotropic character. To enable a comparison, the same requirement also applies for the current study. According to Laws and Livesey [17], a constant ratio of mesh size and bar diameter of H/d = 5 are advantageous to generate elevated level of turbulence of high isotropic character at a sufficient distance from the grid . Figure 8 and Table 1 show the used grids for the presented study, including relevant design parameters.

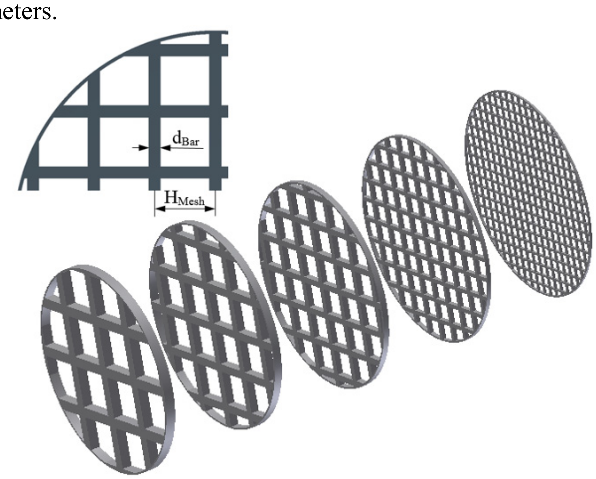

FIG. 8 TESTED BIPLANE SQUARE GRIDS WITH CONSTANT BAR-TO-MESH RATIO H/D = 5 [17].

TABLE 1 GRID NOMENCLATURE AND PARAMETERS OF TESTED GRIDS

Type	Unit	G_{00}	G_{01}	G_{02}	G_{03}	G_{04}	G_{05}
d_{Bar}	[mm]	--	20	16	12	8	4
H_{Mesh}	[mm]	--	100	80	60	40	20
H/d	[--]	--	5	5	5	5	5

 Copyright © 2018 ASME

Downloaded from https://asmedigitalcollection.asme.org/GT/proceedings-pdf/GT2018/50985/V001T09A002/3768152/v001t09a002-gt2018-75369.pdf by guest on 21 July 2020

For obtaining data on the local distribution of the free stream velocity and the grid-generated turbulence in the duct, 1-D hot wire measurements were conducted. A rotating channel (Figure 9) was implemented in the test rig, where the hot wire probe was mounted and traversed in the radial direction from duct-wall to the centre of the duct. Over the measurement duration of 60 seconds for each radial position, the channel rotated by 360 deg at constant velocity normal to the measurement direction of the hot wire probe, covering the full angular path. The hot wire data with a spectral resolution of up to 10 kHz was averaged in angular steps of 10 deg or over 53690 samples, respectively. The total measurement uncertainty, taking into account the calibration process, linearization errors, the A/D conversion, probe positioning uncertainties as well as variations in temperature, ambient pressure and humidity sums up to be 2% for the measured velocity [18]. The turbulence grids were located 0.3 m upstream of the probe location, enabling the generated vortices to break down and mix towards isotropy. The probe location was chosen according to the imaginary position of the fan during the aeroacoustic experiments to be conducted.

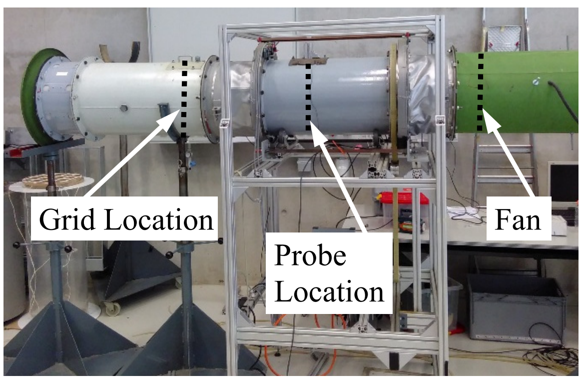

FIG. 9 ROTATING CHANNEL, MOUNTED AT INLET SECTION OF TEST RIG. ROTATIONAL SPEED $2 \cdot \pi$ MIN^{-1}

Figure 10 exemplarily shows results of the velocity profile in the duct with the features of the classical turbulent velocity profile in form of high gradients close to the wall. With grid, the profile appears to be of more uniform character than without, where the grid might act, apart from generating turbulence, as flow straightener, especially stabilising the outer regions, where the boundary layer is located. Nevertheless, the wavy shape of the G_{01} velocity profile hint at the influence of the grid bars, located 0.3 m upstream. Overall, the profiles show a reasonable good homogeneity and are rated to be sufficient for the intended purpose.

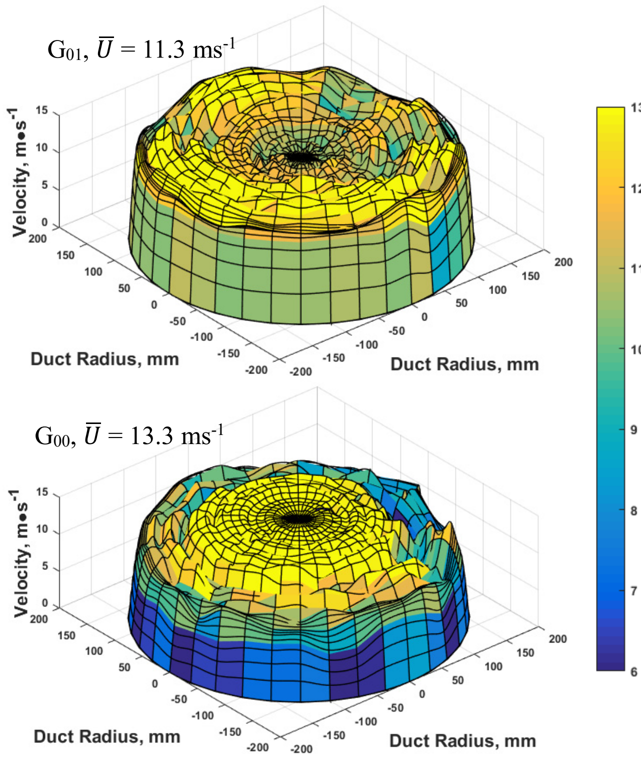

FIG. 10 LOCAL VELOCITY PROFILE IN THE DUCT, EQUIDISTANT STEP WIDTH OF 10 DEG, GRID G_{01} VS. G_{00}

Moving the focus towards the turbulence intensity, a similar pattern as for the velocity profiles can be observed (Figure 11). For the grid G_{01}, turbulence intensities of up to 20% are achieved, showing a uniform distribution in the centre of the duct. Towards the outer regions, a significant increase of the turbulence intensity is visible which can be clearly assigned to the decreasing denominator in form of the mean velocity due to the no-slip condition at the wall. As can be expected from the velocity distribution of the no-grid case (G_{00}), the related turbulence profile shows similar non-uniformities, which are mainly due to the influence of the mean velocity and not due to changes in the fluctuating quantity.

$$Tu = \frac{\sqrt{u'^2}}{\overline{U}} \qquad (2)$$

Copyright © 2018 ASME

Downloaded from https://asmedigitalcollection.asme.org/GT/proceedings-pdf/GT2018/50985/V001T09A002/3768152/v001t09a002-gt2018-75369.pdf by guest on 21 July 2020

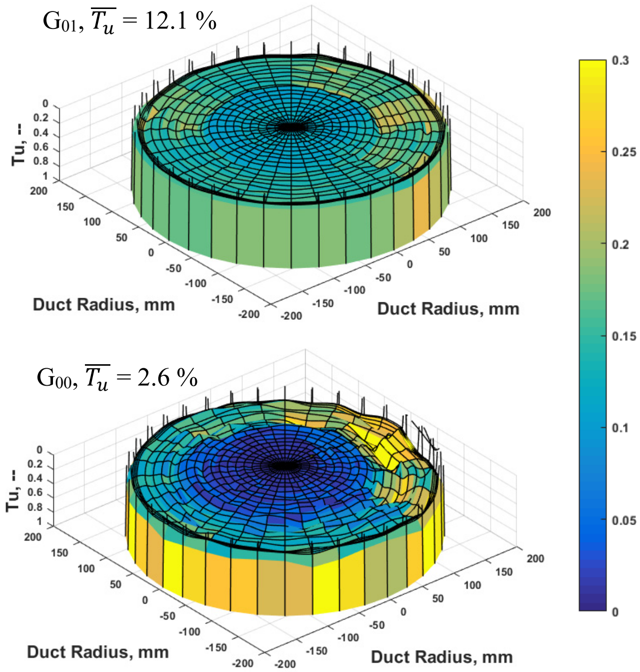

FIG. 11 LOCAL TURBULENCE PROFILE IN THE DUCT, EQUIDISTANT STEP WIDTH OF 10 DEG, GRID G_{01} VS. G_{00}

In order to obtain representative values for each grid, the gathered data was averaged over a radius of 0.15 m to avoid influences by the wall boundary layer. As mentioned earlier, the hot wire probe is located 0.3 m downstream of the turbulence grids. As Table 2 clearly indicates, the turbulence intensity follows the model by Laws and Livesey [17], predicting the most elevated turbulence at maximum mesh size and bar diameter (grid G_{01}). Moreover, the trend of the standard deviation indicates that the higher intensities are mainly due to an increase of the fluctuating quantity and not of the mean velocity. In summary, the generated incoming turbulence for the rotor blades to be analysed can be stated to be in a range of 3.7% ≤ Tu ≤ 12.1%.

TABLE 2 MEAN VALUES OF VELOCITY, TURBULENCE INTENSITY AND STANDARD DEVIATION σ OF THE TESTED TURBULENCE GRIDS

Type	U_{Mean} [m·s^{-1}]	Tu_{Mean} [--]	σ_{Mean} [m·s^{-1}]
G_{01}	11.27	0.121	1.36
G_{02}	11.97	0.097	1.15
G_{03}	11.77	0.078	0.90
G_{04}	11.58	0.059	0.67
G_{05}	12.19	0.037	0.43
G_{00}	13.32	0.026	0.35

As Equation 2 already indicates, the turbulence and thus the fluctuations of the velocity are assumed constant in all spatial directions (constant longitudinal to transversal velocity ratio), leading to an isotropic turbulence intensity. This is of high importance because the turbulent structures are impinging in circumferential direction on the fan blades rather than in the main flow direction. At given isotropy, the measured turbulence in mean flow direction can be equated with the turbulence in circumferential direction and provide a scale of the turbulent inflow conditions at the blade leading edges. However, Laws and Livesey [17] state a minimum distance of roughly ten times the mesh diameter between grid and measurement location to approach isotropic conditions. In the conducted experiments, the coarsest grids G_{01} and G_{02} would require distances of 1.0 m or 0.8 m, respectively, to fulfil this condition. Lower distances might lead to unacceptable downstream inhomogeneities. Therefore, spectral analysis of the 1-D hot wire signals was conducted and compared to the turbulent energy spectra of *von Kármán* and *Liepmann* for longitudinal isotropic turbulence in Equation 3. To take into account the dilution in the high-frequency region, the correction function by Rozenberg [19] (Eq. 4) was applied. Figure 12 shows the power spectral density of the turbulent energy, scaled with the mean flow velocity and plotted over the non-dimensional Strouhal number. Data sets of Grid G_{00} (without grid), G_{01} and G_{02} are analysed at radial positions of $0.15 \leq R_{Duct} \leq 0.198$, starting at mid-span of the fan blades (R = 0.15 m) towards the wall region of the duct (R = 0.198 m). The results demonstrate, that the turbulence model agrees well with the measurements although larger deviations occur close to the wall, especially at high frequencies. A similar trend is observed when increasing the grid dimensions ($G_{00} \rightarrow G_{02} \rightarrow G_{01}$) where high-frequency deviations become more prominent. The turbulent cascade theory describes the turbulent energy to scale with $f^{-5/3}$ in the inertial range and f^{-7} in the dissipation range what can be confirmed for the former range while a diffuse transition to the latter region is observed. Generally, the turbulence intensity can be shown to be of near-isotropic nature even for the coarse grids with large mesh widths.

$$\Phi_{uu}^{L}(\omega) = \frac{\overline{u'^2}\Lambda_{uu}}{\pi U_0} \cdot \frac{1}{1 + K_x^2 {\Lambda_{uu}}^2} \cdot G_{Kolm.} \tag{3}$$

$$G_{Kolm.} = exp\left(\left(-{}^{9}/_{4}\right) \cdot \left({}^{K_x}/_{K_\eta}\right)^2\right) \tag{4}$$

Downloaded from https://asmedigitalcollection.asme.org/GT/proceedings-pdf/GT2018/50985/V001T09A002/3768152/v001t09a002-gt2018-75369.pdf by guest on 21 July 2020

Copyright © 2018 ASME

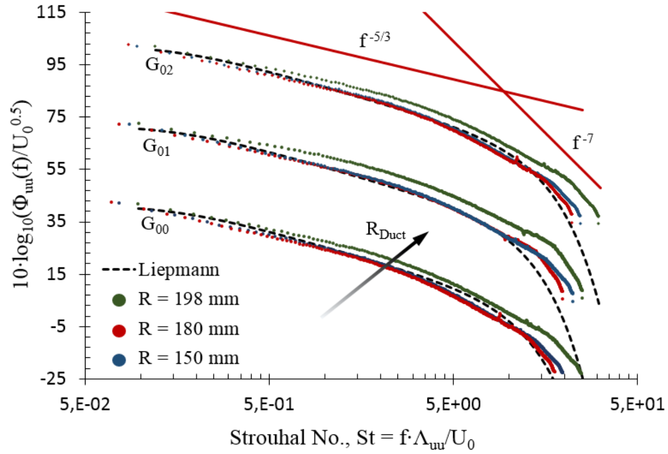

FIG. 12 POWER SPECTRAL DENSITY OF GRID-DEPENDENT TURBULENT ENERGY VS. STROUHAL NUMBER AT DUCT RADIUS R = 198, 180 AND 150 MM. DATA SET OF G_{00} AND G_{02} SHIFTED BY -30 DB AND +30 DB, RESPECTIVELY.

LEADING EDGE SERRATIONS

As already described in section *Rotor Design*, interchangeable rotor blades with leading edge serration of various parameters (Figure 1) were tested in terms of aeroacoustics and aerodynamics. According to the extensive preliminary studies of rigidly mounted serrations [2,6,20,21] the parameters and dimensions of the serrations were adopted and scaled to the current setup, where the aerofoil chord length was the definitive parameter. The maximum serration amplitude was limited to one-third of the aerofoil chord length.

The absolute values of the tested cases are listed in Table 3. It is important to note, that the serrations are cut into the aerofoil main body, keeping the maximum chord length (C = 75 mm) constant. This leads to a slight reduction in the aerofoil surface, affecting the aerodynamic performance. On the other hand, keeping the aerofoil surface constant would lead to a serration-dependent rotor solidity, possibly leading to hardly controllable influences of blade interaction.

TABLE 3 TESTED SERRATION PARAMETERS

Type	Amplitude A [mm]	Wavelength λ [mm]	Max. Chord C [mm]
BSLN	--	--	75
A22λ22	22	22	75
A22λ8	22	8	75
A4λ22	4	22	75
A4λ8	4	8	75

The rotor with straight and serrated leading edges was tested at fixed operation conditions, defined by the rotational speed of RPM = 1530 min^{-1}, the flow rate Q = 1.3 m^3s^{-1} and a pressure rise from suction to discharge side of $\Delta p = 96$ Pa for the baseline case. Yet the presented test rig enables an analysis of the full fan characteristic diagram in terms of aerodynamics, what will be the focus of upcoming studies. Figure 13 and Figure 14 show the rotor with mounted blades of the serrated cases to test as well as the rotor mounted in the duct (Baseline vs. A22λ8).

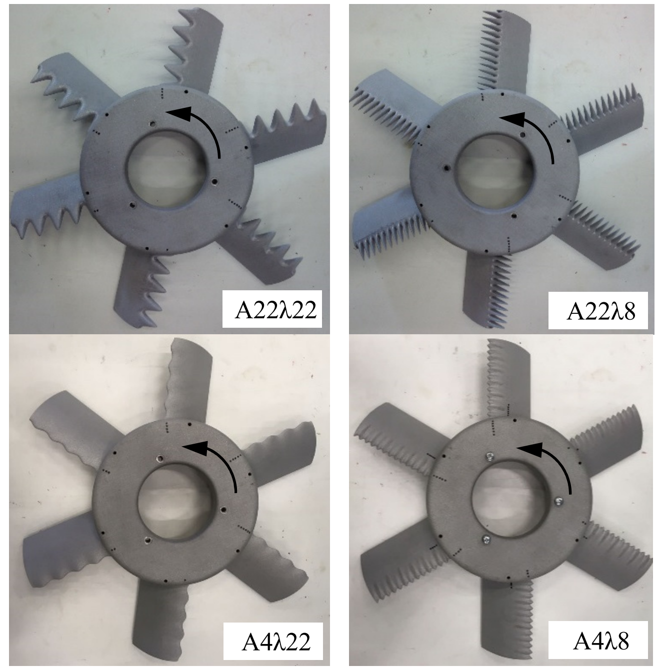

FIG. 13 ROTOR WITH TESTED SERRATED CASES

FIG. 14 DUCT-MOUNTED ROTOR WITH BASELINE VS. A22λ8 CASE

KEY-FINDNGS

With the aim of proving the concept of serrated rotors, all serrated cases have been tested at a single operation point but with all predefined turbulence grids. The aeroacoustic signature was measured via microphone and turbulence screen, approximately x/D = 12.75 downstream of the rotor while the aerodynamic performance in terms of pressure rise and volume flow was recorded simultaneously. Figure 15 shows the acoustic signature of the baseline case at given operation conditions. Based on the given information on rotor, point of operation and e-motor, it is already possible to describe several significant acoustic phenomena.

Downloaded from https://asmedigitalcollection.asme.org/GT/proceedings-pdf/GT2018/50985/V001T09A002/3768152/v001t09a002-gt2018-75369.pdf by guest on 21 July 2020

Copyright © 2018 ASME

The first peak in the spectrum at f_0 = 25.57 Hz (1534 min^{-1}) represents the fundamental frequency of the rotating system. Taking into account the six blades of the rotor yields the blade passing frequency to be at f_{BPF} = 155 Hz. Due to slight variations in amplitude and frequency of the BPF several harmonics occur in the spectrum as well. In addition, the 24^{th} order (or the 4^{th} BPF) of the fundamental frequency exhibits a significant amplitude, which is due to the 24 coils of the e-motor. Finally, with a duct diameter of D = 0.4 m the cut-on frequency (first duct mode) was determined to be $f_{1,0}$ = 501 Hz (Eq. 5).

$$f_{1,0} = 0.586 \frac{c}{D} \sqrt{1 - \left(\frac{U}{c}\right)^2} \tag{5}$$

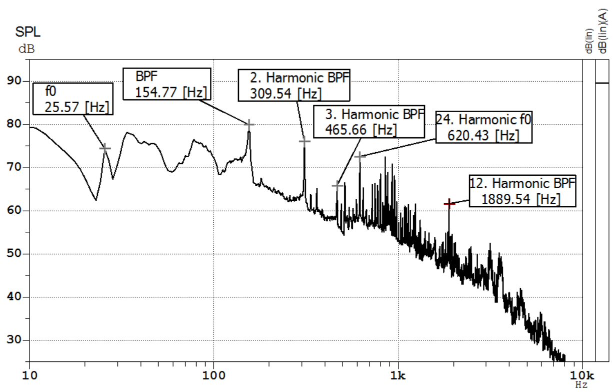

FIG. 15 SOUND PRESSURE SPECTRUM OF BASELINE CONFIGURATION, N = 1530 MIN^{-1}

In a first step, the influence of the different turbulence grids on the acoustic radiation of the fan was investigated. As Figure 16 shows, the overall level increases steadily with increasing the turbulence intensity or the grid size, respectively. This pattern can be mainly assigned to an increase of the broadband noise at frequencies below 2 kHz. During the testing, the operation conditions were kept constant as the fundamental frequency as well as the BPF is matched throughout all measurements. Apparently, grid G_{05} produces high self-noise emissions at high frequencies albeit of no significance concerning the OASPL. The continuous increase of the noise level with increasing the level of turbulence as well as the spectral limitation to lower frequencies indicates the presence of leading edge noise, which typically is of broadband character limited to the lower frequency bands [12].

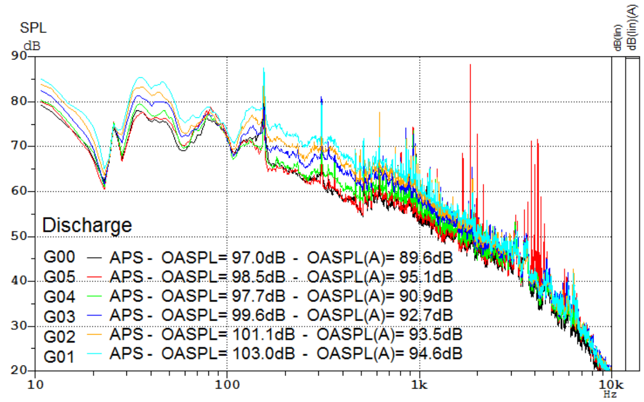

FIG. 16 SOUND PRESSURE SPECTRA, BASELINE CONFIGURATION, INFLUENCE OF GRIDS ON NOISE RADIATION, INDICATED OASPL

Concerning the serrated blades, at maximum incoming turbulence (Tu_{Mean} = 12.1%) the overall sound pressure level reduction turns out to be ΔOASPL = 3.4 dB for the A22λ8 case, followed by ΔOASPL = 2.3 dB for the A22λ22 case and insignificant differences to the baseline for the other serrations (Figure 17). Matching the findings towards the grid-sensitivity of the radiated noise, the noise reduction is mainly limited to frequencies of f ≤ 2 kHz.

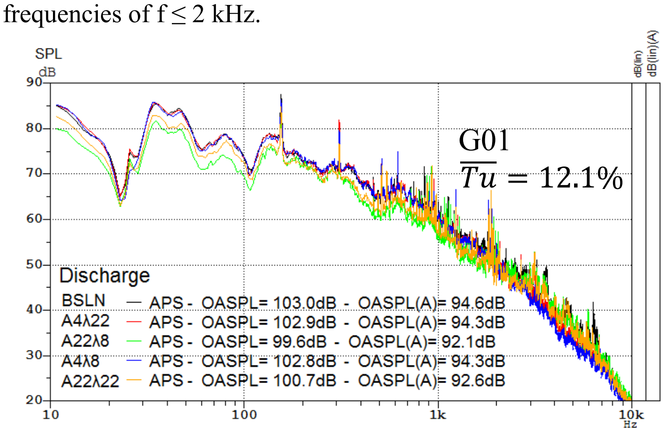

FIG. 17 SOUND PRESSURE SPECTRA GRID G_{01}, N = 1530 MIN^{-1}, TU_{MEAN} = 12.1 %, COMPARISON OF SERRATIONS, INDICATED OASPL

At intermediate levels of the incoming turbulence (Tu_{Mean} = 5.9%) the noise reduction of the A22λ8 case is still on a high level with ΔOASPL = 3.3dB, followed by the significantly reduced noise reduction of ΔOASPL = 0.8 dB for the A22λ22 and ΔOASPL = 1.3 dB for the A4λ8 case (Figure 18). Insignificant differences occur for the other serration. As for the previous measurements, the noise reduction mainly occurs at f ≤ 2 kHz where for the A22λ8 local reductions of up to ΔSPL = 8 dB can be observed.

Downloaded from https://asmedigitalcollection.asme.org/GT/proceedings-pdf/GT2018/50985/V001T09A002/3768152/v001t09a002-gt2018-75369.pdf by guest on 21 July 2020

Copyright © 2018 ASME

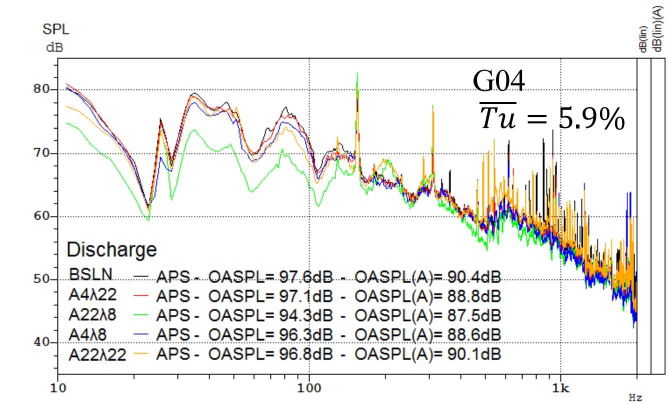

FIG. 18 SOUND PRESSURE SPECTRA GRID G_{04}, N = 1530 MIN^{-1}, TU_{MEAN} = 12.1 %, COMPARISON OF SERRATIONS, INDICATED OASPL

Table 4 shows a summary of the results in terms of overall sound pressure level OASPL and OASPL reduction, applying a low-pass filter of 2 kHz. The A22λ8 serration was found to be most beneficial in terms of aeroacoustics but also show a high sensitivity to the blade alignment. For the tested cases G_{02} and G_{03} a predominant peak occurred at f = 90 Hz due to vibrational problems with the test rig, leading to an increase of the OASPL albeit the broadband signature was lower than the one of the baseline case. In general, the main dependencies, which were found by recent studies, focussing on rigidly mounted aerofoils, can be confirmed. The noise emissions of the fan scale with the level of incoming turbulence. High amplitudes and small wavelengths lead to maximum noise reduction and even at very small amplitudes but small wavelengths noise reduction of up to ΔOASPL = 1.7 dB was observed.

TABLE 4 SUMMARY OF AEROACOUSTIC MEASUREMENT RESULTS, OASPL AND ΔOASPL, (REFERENCE = BASELINE). LOW-PASS FILTER 2 KHZ

	OASPL [dB]	ΔOASPL [dB]	OASPL [dB]	ΔOASPL [dB]	OASPL [dB]	ΔOASPL [dB]	OASPL [dB]	ΔOASPL [dB]	OASPL [dB]	ΔOASPL [dB]
	G01		G02		G03		G04		G05	
BSLN	103,0		101,1		99,6		97,6		98,4	
A4λ22	102,9	**0,1**	100,8	**0,3**	99,4	**0,2**	97,1	**0,5**	97,3	**1,1**
A22λ8	99,6	**3,4**	106,0	-4,9	105,9	-6,3	94,3	**3,3**	96,5	**1,9**
A4λ8	102,8	**0,2**	101,2	**-0,1**	99,0	**0,6**	96,3	**1,3**	96,7	**1,7**
A22λ22	100,7	**2,3**	99,6	**1,5**	98,3	**1,3**	96,8	**0,8**	96,7	**1,7**

Recent studies often focussed on either the aeroacoustic or the aerodynamic performance of serrated leading edges but for practical application both fields have to be taken into account. Thus, the aerodynamic features of each tested rotor configuration were analysed. As expected, significant grid-dependent pressure losses are observed, where grids with large bar and mesh diameter are causing a higher impact (G_{01}) than those with small dimensions (G_{05}). This becomes already visible by analysing the obtained velocity distributions, where, compared to the standard case, a clear reduction of the axial flow velocity was observed for all grids (Table 2). However, comparing the baseline case with the tested cases in terms of serrations reveals clear dependencies (Tables 5 + 6). For all tested grids, the differences in pressure loss and flow rate follow the same serration-dependent tendencies at highly similar dimensions, where the serration amplitude turns out to be the main influencing factor. At small amplitudes the differences in aerodynamics are of negligible impact or even show (e.g. for A4λ22) an improved aerodynamic performance, compared to the baseline case. However, serrations with amplitudes cut deep into the blades' main body (30% of the chord) exhibit pressure and flow rate losses of up to 17% or 10%, respectively. When compared directly, assigning the aerodynamic performance to the aeroacoustic noise reduction capabilities, hints to the classic noise-reduction dilemma of opposing trends even though the design point of the serrated fans might be altered.

Results of a preliminary study on the aerodynamic performance of serrated aerofoils [6,22] show a significant influence of the serration amplitude but not of the wavelength on the resulting lift coefficients. At maximum amplitude (one-third of chord), the lift coefficients dropped by 18% compared to the baseline case. The maximum lift-to-drag ratio, however, was still dominated by the serration amplitude but also influenced by the wavelength, where maximum wavelengths and minimum amplitudes lead to the highest performance. Moreover, the reduced surface area, compared to the baseline, was found not to be the only cause of the reduced lift performance. This observed behaviour seems to be in agreement with the current findings where the blades with the highest amplitudes and smallest wavelengths show the highest drop in pressure and volume flow.

TABLE 5 AERODYNAMIC MEASUREMENT RESULTS, GRID G_{00}, COMPARISON OF SERRATIONS, INDICATION OF DEVIATION FROM BASELINE CASE

Grid G_{00}	Δp Fan [Pa]	Dev Δp [%]	Q [m³s⁻¹]	Dev Q [%]
Baseline	96.1	--	1.29	--
A4λ8	95.7	0	1.28	-1
A4 λ 22	97.2	1	1.28	-1
A22 λ 8	80.0	-17	1.17	-10
A22 λ 22	86.0	-10	1.21	-7

TABLE 6 AERODYNAMIC MEASUREMENT RESULTS, GRID G_{01}, COMPARISON OF SERRATIONS, INDICATION OF DEVIATION FROM BASELINE CASE

Grid G_{01}	Δp Fan [Pa]	Dev Δp [%]	Q [m³s⁻¹]	Dev Q [%]
Baseline	67.5	--	1.08	--
A4 λ 8	67.7	0	1.06	-2
A4 λ 22	68.1	1	1.06	-2
A22 λ 8	54.4	-19	0.95	-12
A22 λ 22	58.4	-14	1.00	-8

With the purpose of comparing the baseline and the A22λ8 case at equal aerodynamic operation conditions, the RPM of the latter case was adjusted from 1534 min^{-1} to 1696 min^{-1} to match

Copyright © 2018 ASME

Downloaded from https://asmedigitalcollection.asme.org/GT/proceedings-pdf/GT2018/50985/V001T09A002/3768152/v001t09a002-gt2018-75369.pdf by guest on 21 July 2020

the Δp of the baseline case. Even though the rotor is at a higher speed, the A22λ8 case still exhibits lower acoustic levels than the baseline.

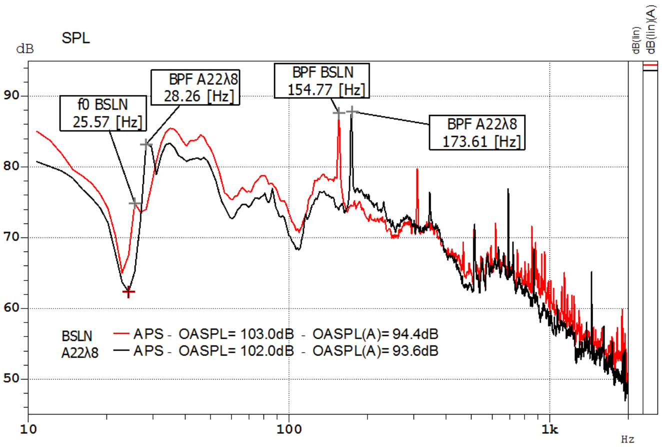

FIG. 19 SOUND PRESSURE SPECTRUM, GRID G_{01}, BASELINE VS. A22λ8 CASE. CONSTANT PRESSURE RISE ΔP = 67.5 PA

CONCLUSIONS

A test rig according to ISO 5136 was adopted and modified with the aim of analysing low-speed axial fans. A rotor with interchangeable blades was designed to analyse serrated leading edges and allow a variation of several parameters such as the stagger angle, the blade design (sweep, skewness, dihedral …), the serration design (amplitude, wavelength …) and the rotational speed. Moreover, the defined test rig allows for an analysis of both, aerodynamic and aeroacoustic performance for the whole fan characteristic diagram. As a *Proof-Of-Concept*, first measurements were conducted with a simple blade geometry for a selected set of serrations at different incoming turbulence intensities. The results obtained allow the current paper to reach the following conclusions:

– The provided detailed information of the velocity and turbulence distribution show homogeneous profiles for the employed turbulence grids and can be taken into account when analysing the radiated noise and the aerodynamic characteristics.

– Reasonable fit to Liepmanns turbulence model, indicating near-isotropic conditions of the turbulence for the tested grids, with reducing isotropy towards the regions close to the wall. Thus, the streamwise turbulence can be assumed equal to the turbulent structures, impinging on the rotor blades in circumferential direction.

– The baseline rotor was shown to be sensitive to incoming turbulence, resulting in broadband noise radiation, primary at $f \leq 2$ kHz. The OASPL scales with the magnitude of the incoming turbulence.

– The noise reduction due to serrated leading edges was found to be of broadband character, mainly limited to $f \leq 2$ kHz.

– Influence of serration amplitude seems to be dominant for noise reduction capability (max. overall noise reduction ΔOASPL = 3.4 dB). The wavelength seems to be of relevance only in small margins but, in principle, small wavelengths are beneficial.

– Clear effect of amplitude and wavelength on aerodynamic performance. High amplitudes combined with small wavelengths lead to significant drop in pressure rise and flow rate where small amplitudes, combined with small wavelengths, lead to equivalent aerodynamics but only little noise reduction (ΔOASPL = 1.4dB).

OUTLOOK/ DISCUSSION

The results of the presented preliminary study allude to the effect of leading edge serrations on noise radiation of axial low-speed fans and provide first information on the influence of different parameters. Admittedly, for conclusions that are more general the full aerodynamic performance map needs to be covered by simultaneously monitoring the aeroacoustics. Further studies will and will need to focus on the effect of serrated blades of successively increasing complexity by including blade skewness, sweep and dihedral as well as more complex serration designs. The design of aeroacoustically beneficial serrations while maintaining acceptable aerodynamic performance poses one of the main challenges in this field of research.

NOMENCLATURE

Λ_{uu}	integral length scale [m]
Φ_{uu}^{L}	turbulent energy [dB/Hz]
ω	angular frequency [s^{-1}]
K_x	specific wave number [m^{-1}]
K_η	high-frequency roll-off constant
$G_{Kolm.}$	spectral dilution factor [--]
U_0	mean flow velocity [ms^{-1}]
u'	velocity fluctuation [ms^{-1}]
c	speed of sound [ms^{-1}]
Tu	turbulence intensity [--]
A	serration amplitude [m]
α	angle of attack [deg]
λ	serration wavelength [m]
D	duct diameter [m]
R	duct radius [m]
f_0	fundamental frequency [Hz]
C	blade chord length [m]
σ_{Mean}	standard deviation [ms^{-1}]
σ_E	equivalent stress [MPa]
σ	rotor solidity [--]
t	blade pitch [--]
c_{1x}, c_{2x}	axial flow velocity [ms^{-1}]
$U_{1,2}$	circumferential velocity [ms^{-1}]
$w_{1,2}$	relative velocity [ms^{-1}]
SPL	sound pressure level [dB]
OASPL	overall sound pressure level [dB]
ΔOASPL	sound pressure level reduction [dB]

Downloaded from https://asmedigitalcollection.asme.org/GT/proceedings-pdf/GT2018/50985/V001T09A002/3768152/v001t09a002-gt2018-75369.pdf by guest on 21 July 2020

Copyright © 2018 ASME

ACKNOWLEDGEMENTS

The authors gratefully acknowledge the support of the B.Eng. and M.Sc. students Nina Balde and Nils Hintzen as well as Tobias Pohlmann from the University of Applied Sciences Duesseldorf.

REFERENCES

[1] Zenger, Florian, Herold, Gert, and Becker, Stefan. “Acoustic Characterization of Forward- and Backward-Skewed Axial Fans under Increased Inflow Turbulence.”. *22nd AIAA/CEAS Aeroacoustics Conference.* Lyon, France. DOI 10.2514/6.2016-2943.

[2] Biedermann, Till M., Chong, Tze Pei, Kameier, Frank, and Paschereit, Christian O. “Statistical-Empirical Modelling of Airfoil Noise Subjected toLeading Edge Serrations.” *AIAA Journal* Volume 55 issue 9 (2017): pp. 3128–3142. DOI 10.2514/1.J055633.

[3] Biedermann, Till M. “Statistical-Empirical Modelling of Aerofoil Noise and PerformanceSubjected to Leading Edge Serrations.” *Internoise* Vol. 2016 (2016).

[4] Chong, Tze Pei, Vathylakis, Alexandros, McEwen, Archie, Kemsley, Foster, Muhammad, Chioma, and Siddiqi, Saarim. “Aeroacoustic and Aerodynamic Performances of an Aerofoil Subjected to Sinusoidal Leading Edges.” (2015). DOI 10.2514/6.2015-2200.

[5] Chaitanya, Paruchuri, Narayanan, S., Joseph, Phillip, and Kim, Jae Wook. “Leading edge serration geometries for significantly enhanced leading edge noise reductions.” *22nd AIAA/CEAS Aeroacoustics Conference* (2016). DOI 10.2514/6.2016-2736.

[6] Biedermann, Till, Kameier, Frank, Koster, Oliver, Schreiber, Denis, Chong, Tze Pei, and Paschereit, C.O. “Polyoptimisation of the Aerodynamic and Aeroacoustic Performance of Aerofoils with Serrated Leading Edges.” *23rd AIAA/CEAS Aeroacoustics Conference* (2017). DOI 10.2514/6.2017-3493.

[7] Biedermann, Till, Chong, Tze Pei, and Kameier, Frank. “Statistical-empirical modelling of aerofoil noise subjected to leading edge serrations and aerodynamic identification of noise reduction mechanisms.” *22nd AIAA/CEAS Aeroacoustics Conference* (2016). DOI 10.2514/6.2016-2757.

[8] ISO, 2008. “Industrial fans – Performance testing using standardized airways (ISO 5801:2007).” ISO 5801.

[9] Zenger, Florian, Renz, Andreas, and Becker, Stefan. “Experimental Investigation of Sound Reduction by Leading Edge Serrations in Axial Fans.” *23rd AIAA/CEAS Aeroacoustics Conference* (2017). DOI 10.2514/6.2017-3387.

[10] Corsini, Alessandro, Delibra, Giovanni, and Sheard, Anthony G. “Leading Edge Bumps in Ventilation Fans.”. *Volume 4: Ceramics; Concentrating Solar Power Plants; Controls, Diagnostics and Instrumentation; Education; Electric Power; Fans and Blowers*: V004T10A007. San Antonio, Texas, USA, Monday 3 June 2013. DOI 10.1115/GT2013-94853.

[11] ISO, 2009. “Acoustics – Determination of sound power radiated into a duct by fans and other air-moving devices – In-duct method (ISO 5136:2003).” ISO 5136.

[12] Carolus, Thomas. *Ventilatoren*. Vieweg+Teubner Verlag, Wiesbaden (2013).

[13] Carolus, Thomas H. and Starzmann, Ralf. “An Aerodynamic Design Methodology for Low Pressure Axial Fans With Integrated Airfoil Polar Prediction.”. *Volume 4: Cycle Innovations; Fans and Blowers; Industrial and Cogeneration; Manufacturing Materials and Metallurgy; Marine; Oil and Gas Applications*: pp. 335–342. Vancouver, British Columbia, Canada, June 6–10, 2011. DOI 10.1115/GT2011-45243.

[14] Wojno, John P., Mueller, Thomas J., and Blake, William K. “Turbulence Ingestion Noise, Part 2: Rotor Aeroacoustic Response to Grid-Generated Turbulence.” *AIAA Journal* Vol. 40 No. 1 (2002): pp. 26–32. DOI 10.2514/2.1637.

[15] Reese, Hauke, Carolus, Thomas, and Kato, Chisachi. “Numerical Prediction of the Aeroacoustic Sound Sources in a Low Pressure Axial Fan with Inflow Distortion.” *Fan Noise 2007* (2007).

[16] Amiet, R. K. “Noise Produced by Turbulent Flow into a Propeller or Helicopter Rotor.” *AIAA Journal* Vol. 15 No. 3 (1977): pp. 307–308. DOI 10.2514/3.63237.

[17] Laws, E. M. and Livesey, J. L. “Flow Through Screens.” *Annual Review of Fluid Mechanics* Vol. 10 No. 1 (1978): pp. 247–266. DOI 10.1146/annurev.fl.10.010178.001335.

[18] Jorgensen, Finn E. “How to measure turbulence with hot-wire anemometers - a practical guide.” Puiblication no. 9040U6151. Dantec Dynamics, Skovlunde, Denmark (2002).

[19] Rozenberg, Yannick. “Modélisation analytique du bruit aérodynamique à largebande des machines tournantes utilisation de calculs moyennés de mécanique des fuides.” Docteur Spécialité Acoustique Dissertation. école centrale de Lyon, Lyon.

[20] Chaitanya, Paruchuri, Narayanan, Subramanian, Joseph, Phillip, Vanderwel, Christina, Kim, Jae Wook, and Ganapathisubramani, Bharathram. “Broadband noise reduction through leading edge serrations on realistic aerofoils.” (2015). DOI 10.2514/6.2015-2202.

[21] Turner, Jacob M. and Kim, Jae Wook. “Aeroacoustic source mechanisms of a wavy leading edge undergoing vortical disturbances.” *Journal of Fluid Mechanics* Vol. 811 (2017): pp. 582–611. DOI 10.1017/jfm.2016.785.

[22] Chong, Tze Pei. “Aerofoil Self Noise Radiation and Aerodynamic Performance Subjected to Leading Edge Serrations.”. Department of Mechanical, Aerospace and Civil Engineering, London, UK (2015).

Downloaded from https://asmedigitalcollection.asme.org/GT/proceedings-pdf/GT2018/50985/V001T09A002/3768152/v001t09a002-gt2018-75369.pdf by guest on 21 July 2020

Copyright © 2018 ASME